

# Updated Sensitivities of the Five STIS L-mode Gratings

Amy M. Jones<sup>1</sup>, Svea Hernandez<sup>1</sup>, Joleen K. Carlberg<sup>1</sup>, Daniel Welty<sup>1</sup>

<sup>1</sup> Space Telescope Science Institute, Baltimore, MD

30 July 2025

---

## ABSTRACT

Re-derivation of the sensitivities of all of the Space Telescope Imaging Spectrograph (STIS) observing modes were required after major updates were introduced to the model atmospheres of the three primary standard stars. The new predicted continuum fluxes were up to 2–3% different from the models used to originally calibrate STIS. This work focuses on the re-derivation of spectral sensitivities for the five STIS low-resolution (L-mode) gratings: G140L, G230L, G230LB, G430L, and G750L, which span wavelengths from the far-ultraviolet through the near infrared. Updated photometric throughput tables were delivered to the Calibration Reference Data System (CRDS) on April 7, 2022 and April 14, 2023, which triggered a recalibration of all historical STIS datasets taken with these modes. The sensitivities derived from each of the standard stars typically agree with one another to better than 1%, though discrepancies as large as 1.5% are found in spectral regions most impacted by hydrogen absorption.

---

## Contents

1. Introduction . . . . .	2
2. CALSPEC Model Updates . . . . .	3
3. STIS Observations . . . . .	4
4. Data Preparation and Sensitivity Derivation . . . . .	6

4.1 Overview of Methodology . . . . .	6
4.2 Detailed Steps . . . . .	7
5. Special Considerations for G750L . . . . .	12
6. Validation of Updated Throughputs . . . . .	13
Acknowledgments . . . . .	17
Change History for STIS ISR 2025-02 . . . . .	17
References . . . . .	18
Appendix A: Observations . . . . .	20

## 1. Introduction

The absolute flux calibration of the Space Telescope Imaging Spectrograph (STIS) relies on the observations and theoretical models of three primary standard stars: the white dwarfs G191-B2B, GD 71, and GD 153 (Bohlin, et al. 1995). Calibrated STIS data from the low resolution gratings, in turn, form the observational backbone of the CALSPEC flux standard library (Bohlin et al. 2014). As advances are made in the theoretical understanding of these primary stars, all data in the CALSPEC library are updated to a self-consistent, state-of-the-art flux scale. See, e.g., the summary of updates on the main CALSPEC website<sup>1</sup>. It is important to note that the STIS data used in the CALSPEC library are reduced with independent software to achieve the highest possible flux precision for those particular data sets and thus can deviate from the standard calibrated data products found in the Barbara A. Mikulski Archive for Space Telescopes (MAST). For a more detailed discussion and comparisons, see Bohlin et al. 2019.

STIS data products delivered by MAST are reduced with the CALSTIS pipeline together with reference files managed by the HST Calibration Reference Data System (CRDS). Changes to either are relatively slow to be adopted as impacts must be tested on the full archive of legacy STIS data spanning the myriad of available observing modes under a variety of observing conditions (e.g., variations in signal-to-noise (S/N), aperture choices, etc.). Therefore, while the primary standard stars have over half a dozen generations of stellar models available, the release of the CALSPEC version 11 models (hereafter v11, described in Section 2) represent the first time the model changes were significant enough to warrant a re-derivation of the sensitivities of STIS’s observing modes. Companion reports document updates to modes not covered in this work, including Carlberg et al. (2022; E140M), Siebert et al. (2024; prioritized pre-SM4 echelle modes), Hernandez et al. (2024; prioritized post-SM4 echelle modes), Fullerton (2025; first-order M modes), and dos Santos et al. (in prep, NUV imaging modes). The status of updated reference file delivery is also

---

<sup>1</sup><https://www.stsci.edu/hst/instrumentation/reference-data-for-calibration-and-tools/astrophysical-catalogs/calspec>

tracked on a dedicated website<sup>2</sup> maintained by the STIS team.

This ISR documents the re-derivation of sensitivities and delivery of PHOTTAB reference files for the five low-resolution (L-mode) STIS gratings. When used together, the L-mode gratings provide a continuous spectral energy distribution (SED) of an object of interest from 1150 Å – 1.027  $\mu$ m with resolutions ranging from 500 to 1440, and they are heavily utilized in the CALSPEC library. The previous PHOTTAB reference files used sensitivities derived nearly two decades ago. The relative changes in these CALSPEC models are summarized in Section 2. The details of the observations and the sensitivity derivations are covered in Sections 3 – 5. We test the resultant flux distributions of standard star data reduced with CALSTIS and new PHOTTAB files relative to the model fluxes in Section 6, and on average we find < 1% residual discrepancies with the models.

## 2. CALSPEC Model Updates

The main motivation for updating the sensitivity of STIS modes is the few percent improvement in the underlying flux models of the three primary white dwarf standard stars, namely G191-B2B, GD 153, and GD 71. These changes encompass advances in the non-local thermodynamical equilibrium (NLTE) modeling of white dwarf atmospheres, updated stellar effective temperature and surface gravity measurements, and an update to the Vega flux used to normalize the models (Bohlin et al 2020). Most of the HST instruments are updating or have updated their sensitivities with the newer CALSPEC models, and these models are labeled as `_mod011` in the CALSPEC library (note that CALSPEC has released v12 as of the time of writing, but the differences between v11 and v12 are minimal). For GD 153 and GD 71, the v11 models are pure hydrogen models from the TMAP2019 grid. The G191-B2B model is a TLUSTY207 line-blanketed model using Rauch et al. (2013) metal abundances. For the STIS L-modes, the previous pipeline sensitivities were derived using a combination of v4 (`_mod004`, for GD 153 and G191-B2B) and v5 (`_mod005`, for GD 71) CALSPEC models. These older models relied on TLUSTY pure hydrogen NLTE models for all three primary stars (Bohlin & Gilliland 2004, Bohlin 2002).

Figure 1 shows the previous and current CALSPEC models for the three standard stars over the wavelength range of STIS. The first panel shows fluxes of the previous models in black and the current models in pink, green, and purple (for G191-B2B, GD 153, and GD 71, respectively). The most notable change is the inclusion of metal line absorption in G191-B2B, which leads to strong absorption features in the UV below  $\sim$  2000 Å. The second panel shows the ratios of the newer models over the previously used models, excluding the forest of absorption features in G191-B2B for clarity. The overall differences are small, ranging from

---

<sup>2</sup><https://www.stsci.edu/hst/instrumentation/stis/flux-recalibration>

Table 1. Summary of observations used

Mode	Spectral range Å	Number of observations		
		GD71	GD153	G191B2B
G140L	1150–1730	28	23	...
G230L	1570–3180	19	19	...
G230LB	1680–3060	19	18	14
G430L	2900–5700	26	24	19
G750L	5240–10270	11	11	11

$\sim 3\%$  increases at the shortest STIS wavelengths for all three stars to  $\pm \sim 1\%$  at the longest STIS wavelengths, depending on the standard star. The average change over the three standard stars is near unity over much of the optical portion of the spectrum.

### 3. STIS Observations

We used data from the full lifetime of STIS, utilizing programs that observed the primary WD standard stars to obtain high S/N for flux calibration purposes. Some of these programs were designed to test sensitivities and calibration for the three STIS detectors, and observed a star at multiple positions across the detector. A few other programs were designed to cross calibrate the Advanced Camera for Surveys (ACS) with STIS, and the more recent programs were part of a regular calibration monitoring campaign. The latter observed the three primary standard stars every two cycles. The white dwarfs GD 71 and GD 153 were observed with all 5 L-modes, whereas G191-B2B was observed only with the CCD L-modes (G230LB, G430L, and G750L). G191-B2B is too bright to safely be observed with the L-modes on the MAMA detectors. A summary of the available data for each mode is given in Table 1. A more detailed list of all the observations from these programs is given in Appendix A Table 2, which provides the target name, observing mode, date and time of the observation, exposure time, observation ID, proposal ID, and any additional notes or flags. All observations used the widest long slit (52x2", the "photometric" slit). CCD observations were taken at both the nominal (middle of the detector) and E1 (near the top of the detector) positions, and the latter have "E1" marked in the notes column of Table 2. Most CCD data were taken with Gain=4 to access the full well depth of the CCD. Data taken at Gain=1 are noted with "G1" in the notes column.

For G140L, the shadow of the repeller wire falls near the nominal position of spectra on the detector. Therefore, STIS's mode select mechanism by default offsets the spectrum  $\sim 3''$  from the detector center. Initially, this offset was

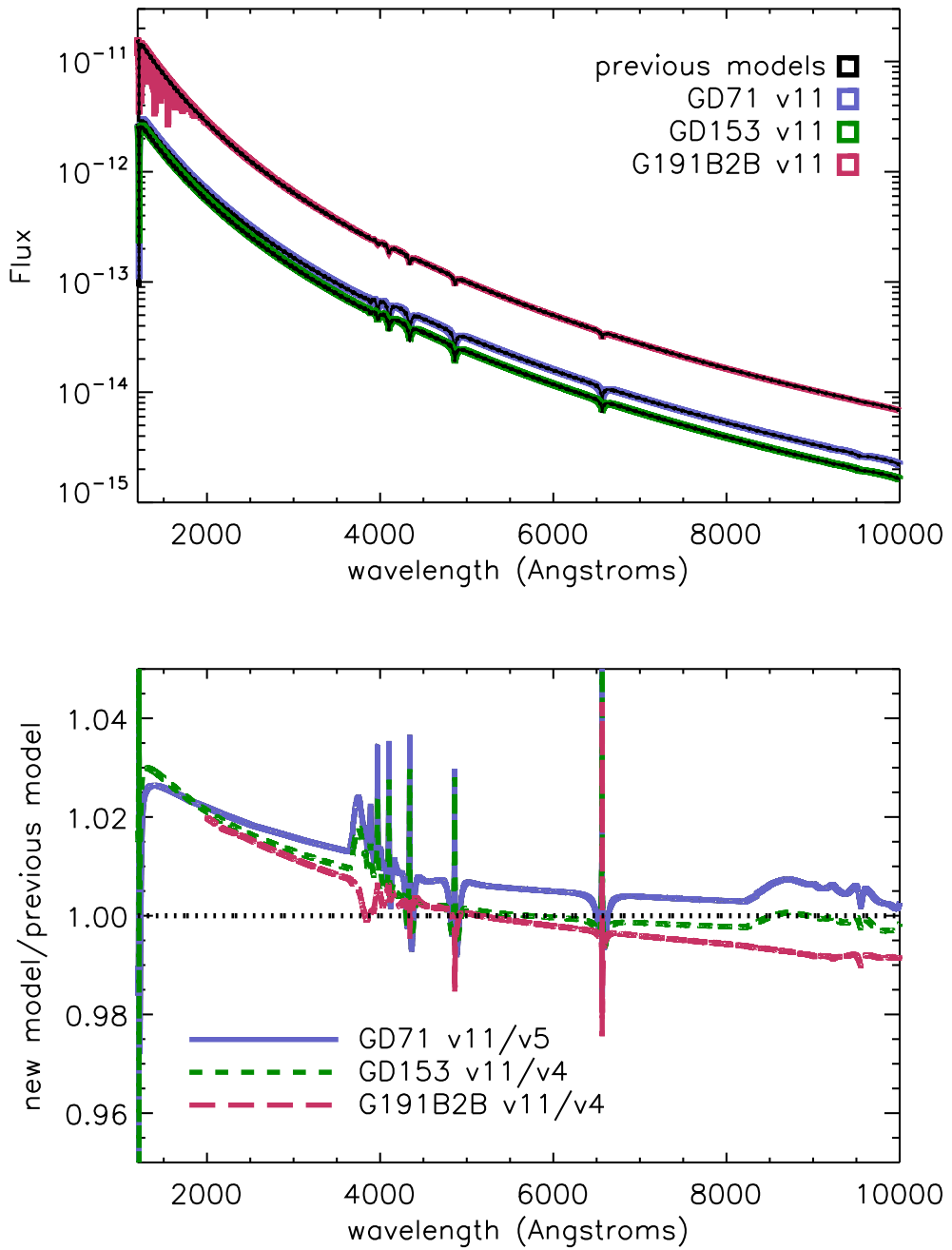


Figure 1. A comparison of the CALSPEC version 11 models of the three primary white dwarf standard stars compared to the older models that were used in the previous determination of the STIS L-mode sensitivities. The comparison is made in both the absolute flux (top) and the ratio (bottom).

towards the top of the detector. In March 1999, the offset was changed to move spectra to the lower part of the detector to avoid the FUV-MAMA glow region. Typically, both G140L and G230L spectra are subject to additional monthly offsets to minimize wear on the detectors. However, special commanding was used to disable these offsets for calibration observations for better repeatability after March 1999. Any MAMA observations observed at non-standard positions on the detector are marked with “P” in the notes column of Table 2.

## 4. Data Preparation and Sensitivity Derivation

### 4.1 Overview of Methodology

The wavelength dependent sensitivity,  $S_\lambda$ , of a given STIS observing mode is the conversion factor between the incidence flux,  $F_\lambda$ , and the resultant count rate on the STIS detectors,  $C_\lambda$ . For a given observation, it is measured for a source with a known model flux,  $F_{\lambda,model}$ , as given in Equation 1.

$$S_{\lambda,obs} = C_{\lambda,obs}/F_{\lambda,model} \quad (1)$$

There are a number of factors that affect the sensitivity of a given observation with STIS that are corrected by the CALSTIS pipeline. The flux calibration step in CALSTIS is performed in calstis6 (McGrath et al. 1999), following the equation in Section 3.4.13 in the STIS Data Handbook (DHB), and reproduced in Equation 2 below.

$$F_{\lambda,calstis} = \left( \frac{1}{R_\lambda} \right) \left( \frac{10^8 \cdot h \cdot c \cdot H}{A_{HST} \cdot T_\lambda \cdot \lambda \cdot \Delta\lambda \cdot f_{GAC}} \right) \left( \frac{G}{f_{TDS} \cdot f_T} \right) C_{\lambda,NET} \quad (2)$$

$F_{\lambda,calstis}$  and  $C_{\lambda,NET}$  are the flux and count rate vectors in the one-dimensional spectra files produced by the CALSTIS pipeline (the “FLUX” and “NET” columns, respectively of the `_x1d.fits` or `_sx1.fits` files).  $R_\lambda$  is the wavelength dependent integrated throughput, which is stored in the PHOTTAB reference file for each optical element. This is the quantity affected by the updates to the primary standard stars’ model fluxes. The terms in the second group of parentheses consists of physical constants, instrument constants, and correction factors contained in other reference files (see the STIS DHB for details). The terms in the third set of parentheses are the gain ( $G$ , CCD only) and correction factors for the time dependent sensitivity ( $f_{TDS}$ ) and the temperature dependent sensitivity ( $f_T$ ), which differ between observations. For CCD data, calstis6 also corrects the net count rates for charge transfer inefficiency (CTI) prior to the flux calibration.

To determine  $R_\lambda$ , we must first correct the net count rate of each standard star observation for observation-specific sensitivity variations. The average corrected net count rates for each primary star are then divided by the updated model fluxes to create an average sensitivity vector per standard star,  $S_{\lambda,star}$ .

Finally,  $R_\lambda$  is calculated from averaging over the sensitivities and scaling by the telescope and instrument constants as in Equation 3 below.

$$R_\lambda = \overline{S_{\lambda,star}} \left( \frac{A_{HST} \cdot T_\lambda \cdot \lambda \cdot \Delta\lambda \cdot f_{GAC}}{10^8 \cdot h \cdot c \cdot H} \right) \quad (3)$$

## 4.2 Detailed Steps

In this work, we used the net count rates in the extracted one-dimensional spectra files produced by the CALSTIS pipeline using the default extraction heights and background regions for each mode. Using the default parameters ensures that the updated absolute flux calibration is optimized for the typical STIS data products in the MAST archive. The NET data have already been corrected for sky background and instrumental effects, such as flat field variation, bias and read noise, dark subtraction, and cosmic ray rejection. However, time ( $f_{TDS}$ ) and temperature ( $f_T$ ) dependent sensitivity changes have not yet been removed nor corrections for CTI for the CCD L-modes and the red halo correction for G750L (as in Equation 2 above). To determine the cumulative effect of these corrections, we run CALSTIS twice – the first with the usual defaults and corrections and the second with setting the primary header keywords TDSTAB to “N/A” and, for CCD modes, CTECORR to “OMIT”. The ratio of the FLUX columns of the resulting pairs of \_x1d files yields the correction factors for the observation-specific sensitivity variations. These correction factors are applied to the NET to correct them to a common STIS epoch and detector temperature. In Figure 2, we use G230LB observations as an example showing the NET count rates for each primary standard before and after applying these corrections and gain factor.

CCD observations are also impacted by cosmic rays. By default, CCD exposures are split into two identical sub-exposures (CRSPLIT=2) to allow for cosmic ray removal in CALSTIS. Occasionally, telescope jitter during the observation can introduce small spatial offsets between the sub-exposures, leading the cosmic ray rejection algorithm to reject substantial valid data in the spectral extraction region as cosmic rays. When the two sub-exposures are combined, the resulting NET count rate will then be systematically low. Following the recommendations in Carlberg (2019) and Hernandez (2021), we inspected the number of cosmic-ray-rejected pixels in the spectral extraction region compared to the full CCD. If the number rejected was higher than 20%, we removed those data from the analysis. For GD71 with G750L, we lowered the threshold to 12% to further remove obvious outliers and bad data. Two G430L and several G750L observations were flagged, and they are marked in the Table 2 as “HCR” (High Cosmic Rays). We did attempt to recover erroneously rejected counts by running ocreject independently and increasing the threshold for cosmic ray rejection. However, this workflow alters the order of the cosmic ray rejection, dark subtraction, and flat fielding compared to running CALSTIS start

to finish, and we found the results to be unreliable (see STIS DHB section 3.5.4 “Improving Cosmic Ray Rejection” for more details). Additionally there were a few observations from this calibration program that were not included because of poor data quality or non-standard observing modes (e.g., using sub-arrays).

G750L spectra are additionally affected by fringing at wavelengths  $> 7000 \text{ \AA}$ , due to interference of multiple reflections of long-wavelength light in the detector. The defringe tool in the stistools package was used to correct fringes, using contemporaneously observed fringe flats. We followed the same procedure described in Hernandez (2021), except when we ran `stistools.x1d.x1d()` after dividing by the fringe flat, we ran it twice, one with the usual defaults and one with the TDS and CTE corrections off, like for G230LB and G430L<sup>3</sup>. We then found the corrected NET count rates from the ratio of the fluxes from the final defringed `_x1d` products.

Once the corrected NET count rates are in hand, the data are placed on a common wavelength scale using a flux conserving interpolation. A heliocentric correction was not applied to each spectrum since this correction is about 100 times smaller than the velocity resolution of the L-modes. All data for a given standard star are then combined with a sigma-clipped mean at each wavelength pixel. This step has the added benefit of removing uncorrected hot pixels and/or cosmic rays missed by the DARKCORR and CRCORR steps of CALSTIS (e.g., the gray spikes in the bottom panel of Figure 2).

---

<sup>3</sup>Note, that at the time of the analysis, the standalone `stistools.x1d.x1d()` behavior was not altered by changing the primary header keyword calibration switches of the data files. Instead one must set the corresponding arguments of the `stistools.x1d.x1d()` task itself, e.g., ‘CTECORR=OMIT’ to alter the calibration.

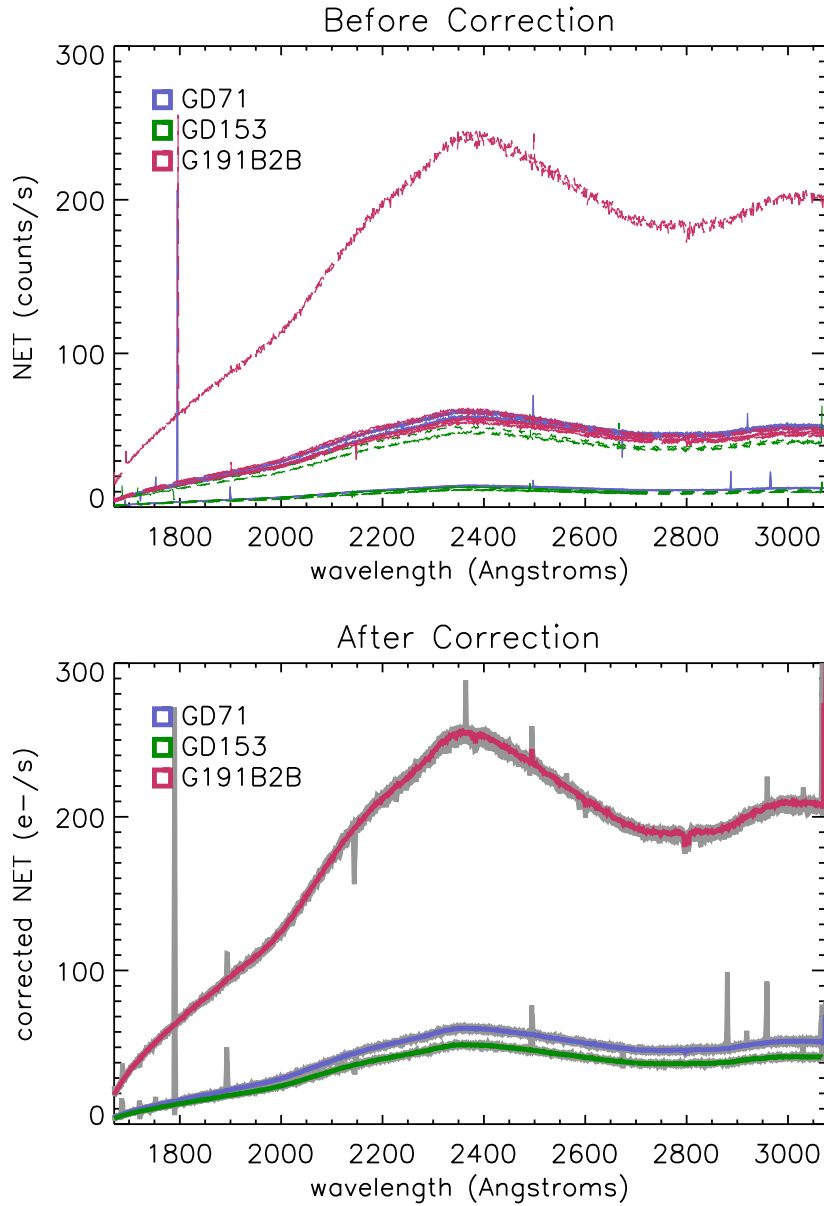


Figure 2. The top panel shows the raw NET count rates of individual G230LB observations of the three primary standards. In the second panel, the NET count rates have been multiplied by a correction factor to account for time and temperature sensitivity variations and converted to electrons per second (taking into account the CCD gain). The individual spectra are now shown in gray with the averages overlaid in color. Most of the spread between observations of a given target is gone.

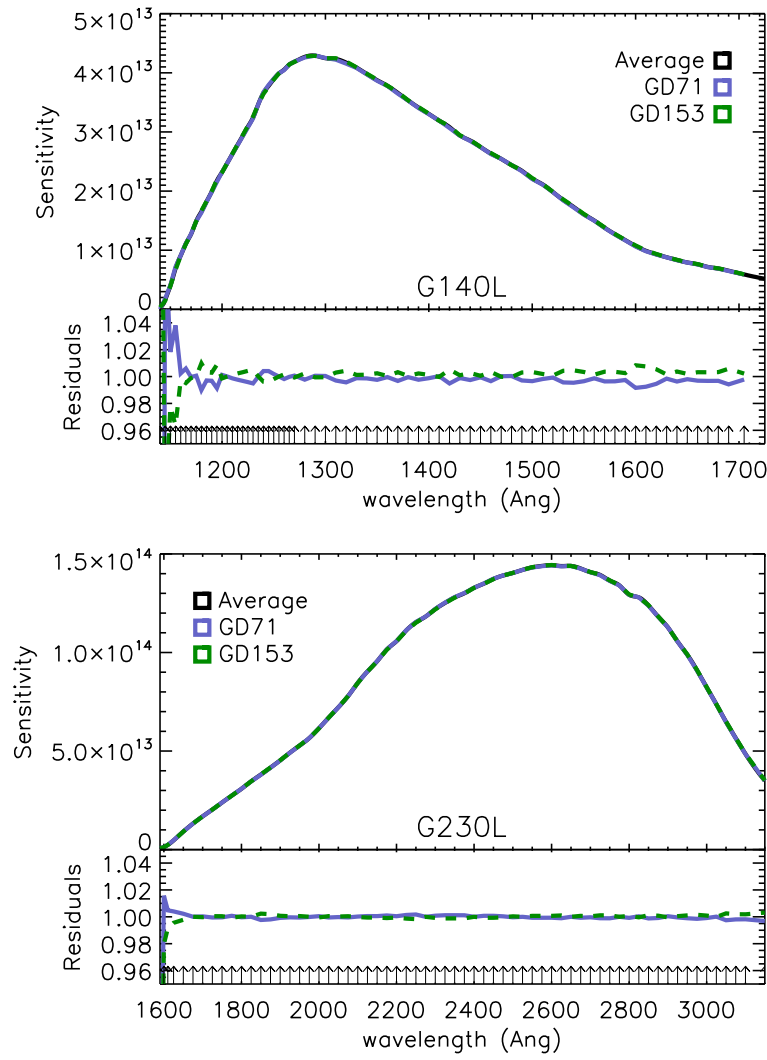


Figure 3. The sensitivities and residuals for each standard star and the average sensitivity for G140L (top) and G230L (bottom). The spline nodes are overlaid at the bottom of each as arrows.

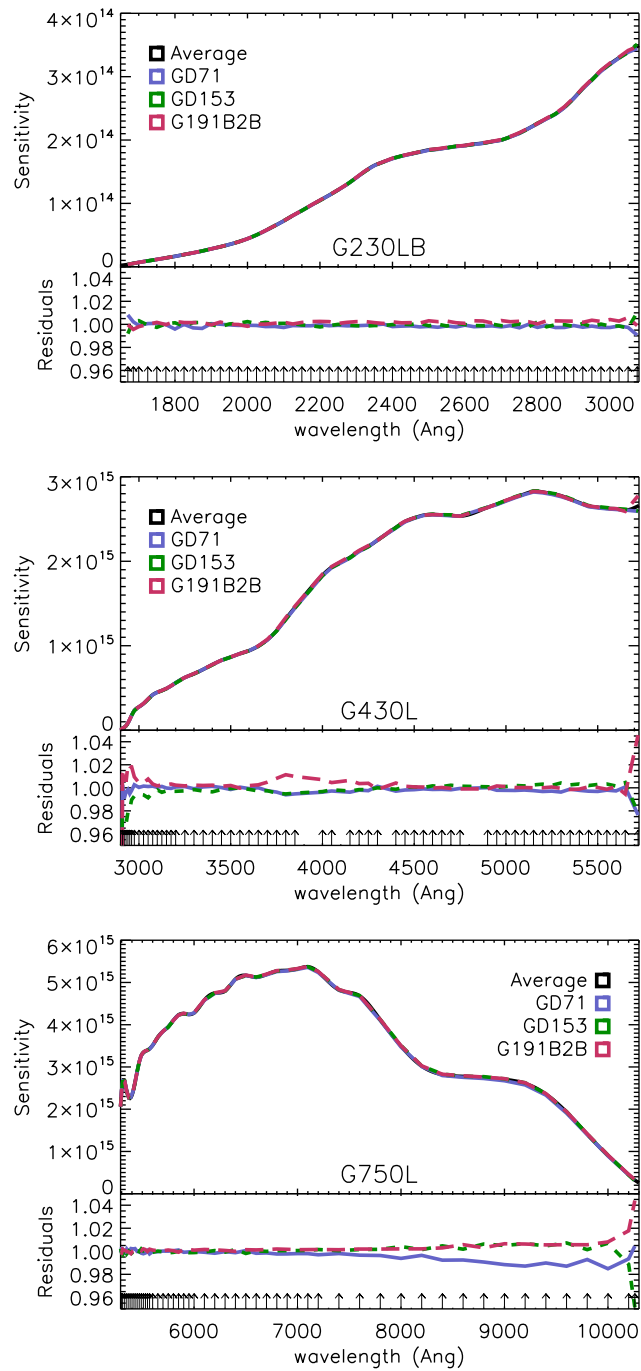


Figure 4. Same as Figure 3 for the 3 CCD gratings.

The sensitivity of each mode ( $S_{\lambda,star}$ ) is first measured for each star by dividing the average corrected NET count rates by the corresponding CALSPEC flux model, which has been similarly interpolated onto the same wavelength grid as the observations. These initial sensitivities are fit with a customized spline for each mode to ensure the curves are finely sampled enough to capture any changes in the sensitivities or model fluxes. The spline nodes are shown as arrows at the bottom of each panel in Figure 3 and Figure 4. Emission or absorption features are masked from the fit, including both the cores and wings of the Hydrogen Lyman and Balmer series lines. This is because the models still do not reproduce these features well. The spline fits for each available primary standard are then averaged together with equal weights to obtain the final sensitivity per observing mode ( $\overline{S_{\lambda,star}}$ ). The sensitivities for each star and the average per mode are shown in Figure 3 and Figure 4. The difference between the star's sensitivity and the average is also shown in the bottom panel for each mode, labeled as the 'Residuals'. The residuals are typically better than 1% over most of the spectral range of each grating, though it rises to  $\sim 2\%$  at the edges. The exception is very red end of G750L where residuals increase to about 4%. See section 5 for more details about G750L.

These average sensitivities per mode, in units of (counts/s)/(ergs/cm<sup>2</sup>/s/Å) are then used to compute integrated throughputs ( $R_{\lambda}$ ) for the PHOTTAB reference files used by CALSTIS. The sensitivities describe the telescope throughput as measured through the 52x2" aperture, which is the mode used in the observations, and extracted using the nominal 7 or 11 pixel extraction box height, depending on the mode. They are then converted to throughput curves, defined as the efficiencies for an infinite aperture and infinite extraction box following the equation in Bostroem et al. (2012). The conversion also takes into account the collecting area of HST. The PHOTTAB is then updated with the new throughputs for these observing modes (see Equation 3).

## 5. Special Considerations for G750L

Updated throughputs for G750L were delivered a year after those for the other four L-mode gratings. There are several factors that complicate the G750L wavelength range, causing a compounding degradation of data quality at longer wavelengths. Already mentioned above are the fringes at wavelengths longer than 7000 Å. Additionally, white dwarfs are fainter at longer wavelengths leading to both lower signal-to-noise (S/N) per observation and longer exposure times, which increase the impact of cosmic rays. In Table 2, observations flagged with 'HCR' occur disproportionately more often for the G750L observations. Only 11 observations of each star were used in our analysis, the least of all the L-modes Table 1.

The point spread function (PSF) of STIS also has a strong wavelength dependence for G750L, where the enclosed energy for the default 7-pixel extraction

height drops below  $\sim 80\%$  redward of  $\sim 8000$  Å (Leitherer & Bohlin 1997). The excess flux in the wings of the PSF at long wavelengths is referred to as the “red halo”. With fractionally more light in the PSF wings, the photometric precision at the longest wavelengths is much more sensitive to focus variations (see, e.g., Proffitt et al., 2017). The CTE correction for G750L also accounts for the red halo (see the STIS DHB Chapter 3.4.6 ‘CTECORR’ and Goudfrooij 2006) to avoid underestimating the number of charge traps filled by electrons outside the extraction box. To minimize these complications, the custom pipeline used by CALSPEC adopts an 11-pixel extraction height for G750L. The CALSTIS pipeline which is the default pipeline, in contrast, adopts a 7 pixel extraction height for all CCD data as an optimal trade-off between achievable S/N and photometric precision for typical moderate S/N STIS spectra (Leitherer & Bohlin 1997). Since our sensitivities will be used by CALSTIS we also maintain a 7 pixel extraction height for consistency. However, we tested a number of variations in how the G750L spectra were extracted prior to the sensitivity derivation, including increasing the extraction height to 11 pixels and re-factoring the CTE correction so that the CTE reference time (2002) would match that used by TDS (1997). None of these variations resulted in significantly different sensitivity shapes. Therefore, we conclude that our method of averaging the sensitivity derivations per standard star and averaging again over all three standard stars is robust to the interplay of fringing, lower S/N, and increased PSF width affecting these wavelengths that lead to the larger residual scatter in Figure 4.

## 6. Validation of Updated Throughputs

We verified the new sensitivities in a few ways. After creating a new PHOTTAB based on the updated sensitivities for each mode, we re-reduced all the data for the primary standard stars through CALSTIS with the new PHOTTAB (including defringing G750L spectra) to compare with the CALSPEC models. The results are shown in Figures 5 and 6 for each L-mode as the re-processed data divided by the models. The fluxes were median smoothed with a 25 pixel kernel. The average spectrum per star per mode is less than 1% different from the model at all wavelengths, except at edges where there is less throughput and signal, at wavelengths  $>8000$  Å (see section 5), and at emission/absorption features where we expect differences between the data and models (see Bohlin et al 2020). The standard deviations are shown as the banded regions and are typically less than 2%. Sharp spikes seen only in the banded region (i.e., very local high standard deviation) typically show up only for the CCD gratings (G230LB, G430L, and G750L) and are likely due to unstable hot pixels that are not optimally removed by the monthly dark file.

In Figures 5 and 6, the sharp spikes in the averages are typically discrepancies in either the narrow metal absorption features of G191-B2B (below  $\sim 2000$  Å in

G230LB, which show up because the models have not been convolved to the STIS spectral resolution) or in the cores of the strong hydrogen absorption features. These include Lyman  $\alpha$  in the G140L passband, the Balmer series (with the exception of Balmer  $\alpha$ ) in the G430L passband, and Balmer  $\alpha$  and Paschen  $\delta$  and higher energy lines in G750L. Broadband discrepancies between the different standard stars arise at the Balmer jump ( $\sim 3647$  Å) and the Paschen bump ( $\sim 8206$  Å), highlighting the limitations of the atmospheric modeling. G191-B2B is the outlier standard star at the Balmer jump, while GD 71 is the outlier at the Paschen jump.

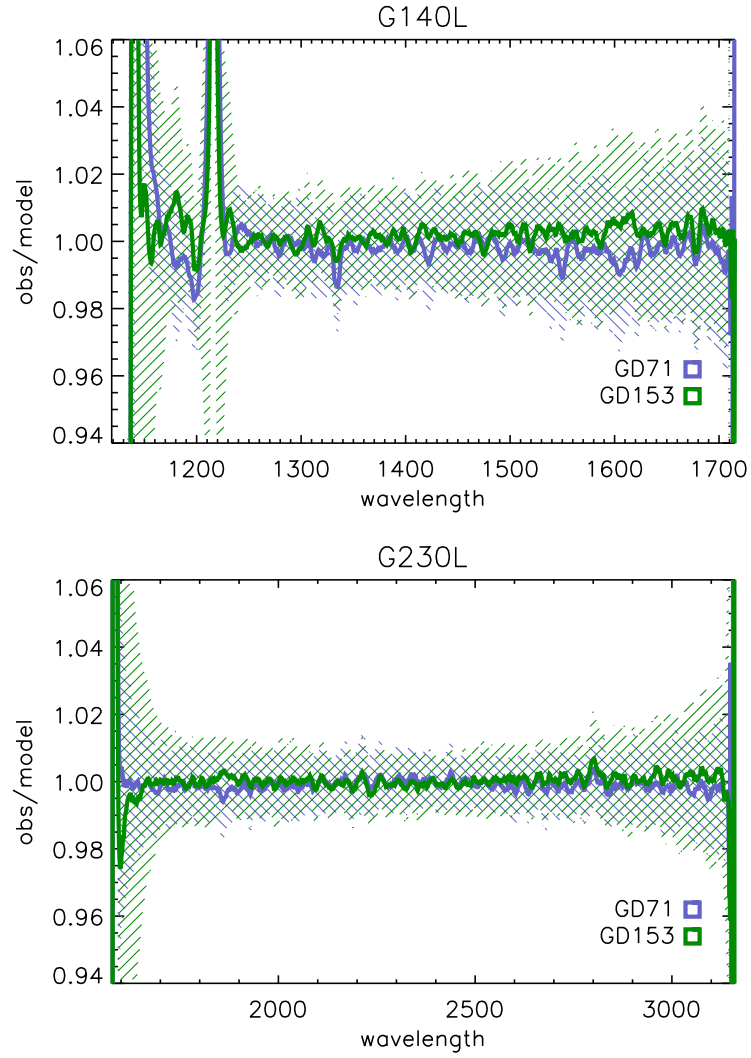


Figure 5. Plots showing the ratio of the smoothed average flux of the data set after being re-run with the updated PHOTTAB over the CALSPEC model for each standard star for the MAMA detectors. The standard deviations are shown as the banded regions. Typically, the re-reduced data agree with the model to better than 1% on average, and within 2% for individual datasets. Exceptions include the grating edges, where S/N is lowest, and in the cores of narrow absorption or emission features (e.g., the Lyman  $\alpha$  line in G140L).

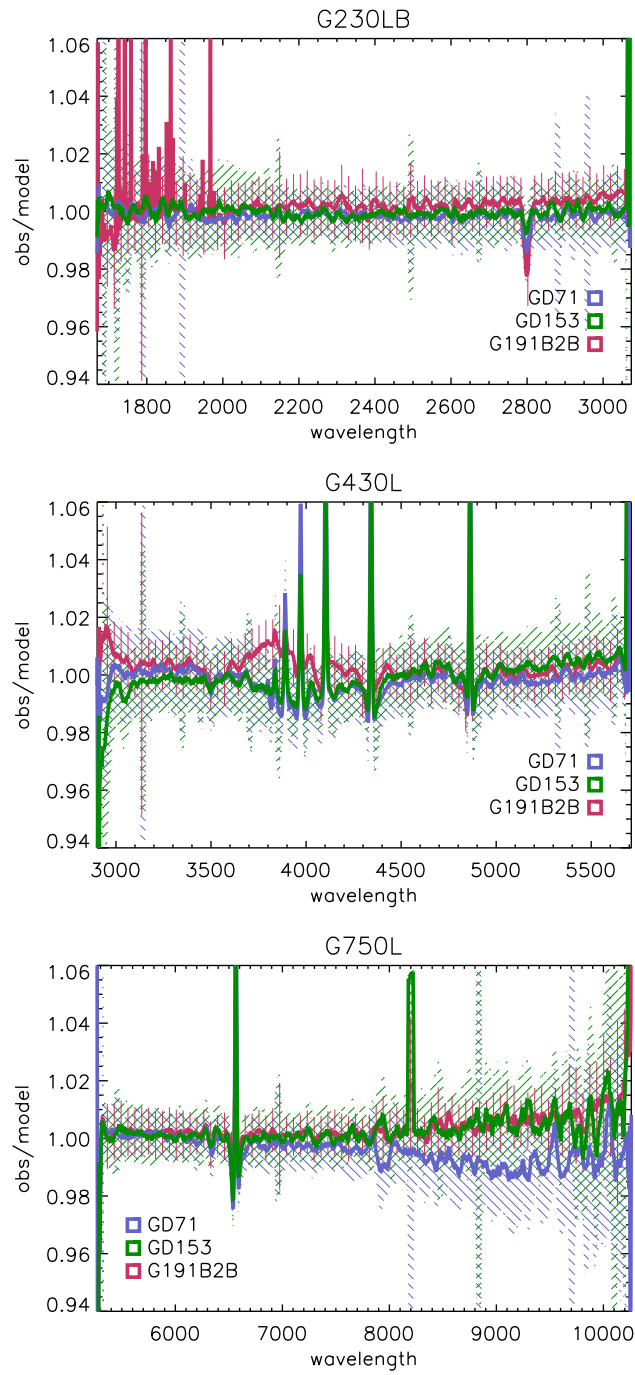


Figure 6. Same as Figure 5 for the 3 CCD gratings. In the optical and near infrared, the broadband discrepancies at the  $\sim 1.5\%$  level between the models are likely due to limitations in the modeling. In G430L data, G191-B2B deviates from other two standards between the Balmer jump ( $\sim 3647 \text{ \AA}$ ) and Balmer  $\delta$  ( $\sim 4341 \text{ \AA}$ ). Similar discrepancies arise for G750L data of GD 71, from the Paschen jump ( $\sim 8206 \text{ \AA}$ ) to beyond the Paschen  $\gamma$  line ( $\sim 10052 \text{ \AA}$ )

We also looked at the regions where the wavelength ranges of some of the L-modes overlap. G230L and G230LB cover a similar wavelength range in the NUV and overlap on the ends with G140L and G430L. G430L and G750L also overlap. These overlapping regions are shown in Figure 7. For clarity, the pixels at the edges were removed since those tend to fluctuate more due to the lower S/N. The average ratio of the fluxes from the re-processed data and the model are shown in different colors for the different gratings, and the stars are plotted with different line styles. There is good agreement between the L-modes, with differences usually less than 1%.

Lastly, for a check independent of the data we used to re-derive the sensitivity, we compare CALSTIS-reduced STIS data of the helium white dwarf WD 0308-565, which is used as a flux standard for the HST/COS instrument (e.g., Miller et al, 2024), to its CALSPEC model. For ease of comparison across the full spectral range of STIS, we retrieved the Hubble Advanced Spectral Product (HASP, Debes et al., 2024) program-level co-added spectra from program IDs 12418 and 16028. Figure 8 shows both the flux comparison of the data compared to the CALSPEC model and the ratio of the data to the model as a function of wavelength for the full wavelength range covered by the five STIS L-mode gratings. The HASP spectral products do not correct for fringing in G750L, which leads to much larger residuals at the longest wavelengths. In the top panel of Figure 8, the model spectra have not been convolved to the (lower) resolution of the STIS spectra, so the cores of deep spectral lines or lines with intrinsically narrow widths show apparent discrepancies with respect to the observations. However, the shapes of the lines with large intrinsic broadening (e.g., between  $\sim$ 3800–5000 Å) are well matched between the models and observations.

In the ratio panel of Figure 8, strong spectral features are masked, and the ratio has been smoothed by a 5 point boxcar filter for visual clarity. Horizontal lines at  $\pm 2\%$  have been plotted to guide the eye. The individual spectra show variations consistent with what was seen in Figures 5 and 6. It is noteworthy that the regions of largest discrepancy coincide with the lowest S/N, particularly at the longest and shortest wavelengths where there is no overlapping wavelength coverage to compensate for the low sensitivity at the grating edges (Figure 3).

## Acknowledgments

The authors are incredibly grateful to Ralph Bohlin for his support, expertise and tireless efforts to maximize STIS's calibration accuracy. We also thank Doug Long for supporting the early stages of this initiative.

## Change History for STIS ISR 2025-02

Version 1: 30 July 2025 - Original Document

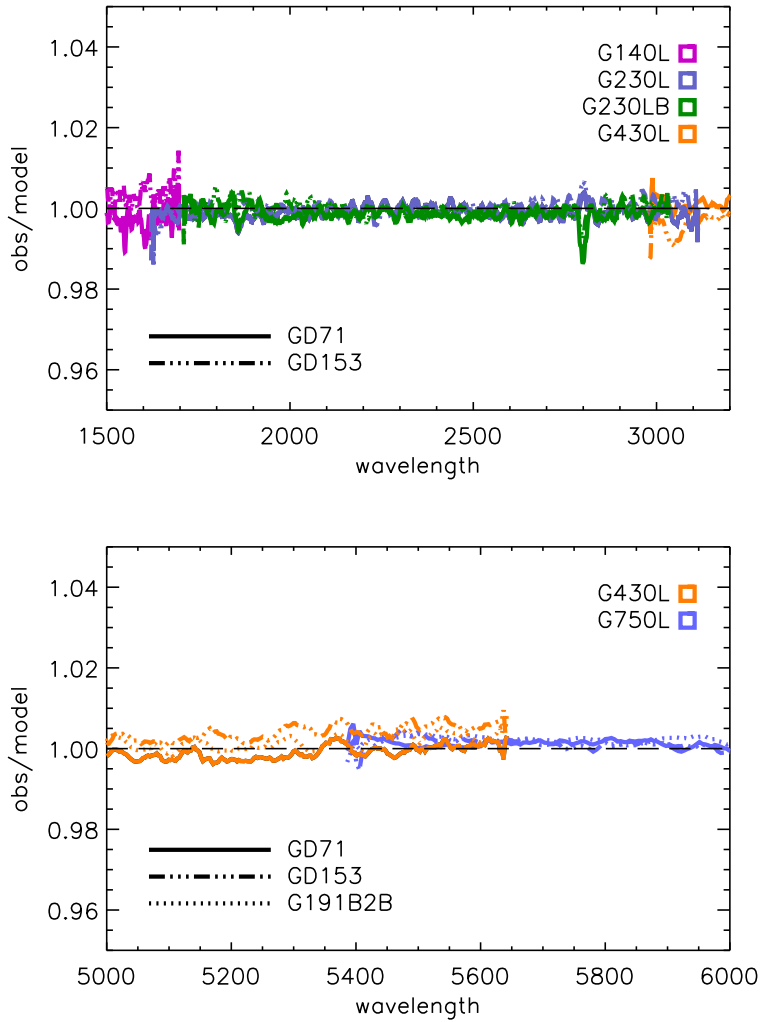


Figure 7. The ratio of the smoothed average flux of the data after re-reducing it with the updated PHOTTAB to the CALSPEC model in wavelength regions where some of the L-mode gratings overlap. The different gratings are shown as the different colors with the standard stars as different line styles. For clarity, the pixels at the edges were removed. There are no systematic differences seen between the different gratings.

## References

Bohlin, R., 2002, HST Calibration Workshop, ed. S. Arribas, A. Koekemoer, & B. Whitmore (Baltimore: STScI), 115

Bohlin, R.C., Colina, L., & Finley, D.S. 1995, AJ, 110, 1316

Bohlin, R. C., Deustua, S. E., & de Rosa, G. 2019, AJ, 158, 211

Bohlin, R. C., Gilliland, R. L., 2004, AJ, 128, 6

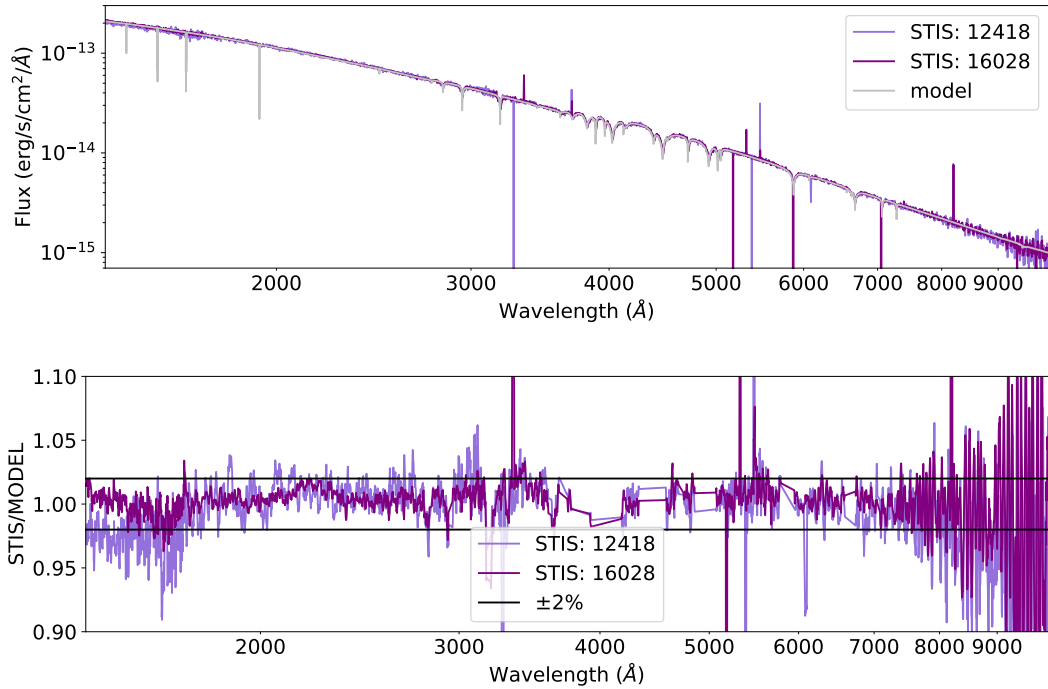


Figure 8. (Top): STIS observations (purple lines) of COS standard star WD 0308-565 from the FUV through near IR compared to the CALSPEC model atmosphere (gray). (Bottom): The same data plotted as a ratio relative to the model, with residuals in deep absorption features removed and the ratio spectrum smoothed with a boxcar filter. The data are HASP co-added spectra from two separate HST observing programs. The long wavelength data have not been defringed. The median S/N for data from program 16028 (dark purple) is 96, while for program 12418 (light purple), the median S/N is only 50.

Bohlin, R. C., Gordon, K. D., & Tremblay, P.-E. 2014, PASP, 126, 711  
 Bohlin, R., Hubeny, I., & Rauch, T. 2020, AJ, 160, 21  
 Bostroem, K. A., Aloisi, A., Bohlin, R., Hodge, P., & Proffitt, C. 2012, STIS Instrument Science Report 2012-01  
 Carlberg, J., 2019, STIS Instrument Science Report 2019-02  
 Carlberg, J., et al., 2022, STIS Instrument Science Report 2022-4  
 Debes, J., et al., 2024, COS Instrument Science Report 2024-01  
 Goudfrooij, P., 2006, STIS Instrument Science Report 2006-03  
 Hernandez, S., 2021, STIS Instrument Science Report 2021-01  
 Hernandez, S., et al., 2024, STIS Instrument Science Report 2024-04  
 Leitherer, C. & Bohlin, R., 1997, STIS Instrument Science Report 1997-13  
 McGrath, M. A., Busko, I., & Hodge, P. 1999, STIS Instrument Science Report 1999-03  
 Miller, L., et al., 2024, COS Instrument Science Report 2024-16

Proffitt, C. R., Monroe, T., & Dressel, L., STIS Instrument Science Report 2017-01

Rauch, T., Werner, K., Bohlin, R., & Kruk, J. W. 2013, A&A, 560, A106

Rickman, E., Brown J., et al., 2024, "STIS Data Handbook", Version 8.0, (Baltimore: STScI)

Siebert, M., et al., STIS Instrument Science Report 2024-02

## Appendix A: Observations

Table 2. STIS Observational Data

Target	Mode	Date (YY-MM-DD)	Time (HH:MM:SS UT)	Exptime (s)	Obs ID	Prop ID	Flags:
G191B2B	G750L	98-02-11	06:04:24	1980.0	o49x07010	7674	HCR
G191B2B	G750L	98-02-26	02:21:52	1980.0	o49x08010	7674	HCR
G191B2B	G230LB	97-10-18	18:27:14	150.0	o4d101010	7805	
G191B2B	G430L	97-10-18	18:35:59	150.0	o4d101020	7805	
G191B2B	G750L	97-10-18	18:44:44	1020.0	o4d101030	7805	
G191B2B	G230LB	97-11-22	19:10:38	150.0	o4d102010	7805	
G191B2B	G430L	97-11-22	19:19:23	150.0	o4d102020	7805	
G191B2B	G750L	97-11-22	19:28:08	1020.0	o4d102030	7805	
G191B2B	G230LB	01-01-20	06:07:25	240.0	o69u05010	8849	
G191B2B	G430L	01-01-20	06:17:46	240.0	o69u05020	8849	
G191B2B	G750L	01-01-20	06:28:07	1200.0	o69u05030	8849	
G191B2B	G230LB	01-02-22	11:18:11	240.0	o69u06010	8849	
G191B2B	G430L	01-02-22	11:28:32	240.0	o69u06020	8849	
G191B2B	G750L	01-02-22	11:38:53	1200.0	o69u06030	8849	
G191B2B	G430L	03-10-29	02:59:11	70.0	o8v203020	10039	G1
G191B2B	G430L	03-10-29	03:49:11	70.0	o8v203030	10039	E1, G1
G191B2B	G230LB	03-10-29	03:56:42	150.0	o8v203040	10039	E1, G1
G191B2B	G230LB	03-10-29	04:01:22	150.0	o8v203050	10039	G1
G191B2B	G750L	03-10-29	04:10:13	290.0	o8v203060	10039	G1
G191B2B	G430L	10-03-15	13:03:29	200.0	obbc07010	11889	E1
G191B2B	G430L	10-03-15	13:08:59	200.0	obbc07020	11889	
G191B2B	G230LB	10-03-15	13:15:55	200.0	obbc07030	11889	
G191B2B	G750L	10-03-15	13:25:35	1310.0	obbc07040	11889	HCR
G191B2B	G430L	11-01-31	04:33:50	200.0	obnf05010	12392	E1
G191B2B	G430L	11-01-31	04:39:20	200.0	obnf05020	12392	
G191B2B	G230LB	11-01-31	04:46:15	200.0	obnf05030	12392	
G191B2B	G750L	11-01-31	04:55:56	1308.0	obnf05040	12392	
G191B2B	G430L	11-11-06	12:47:55	200.0	obvp07010	12737	
G191B2B	G430L	11-11-06	12:53:25	200.0	obvp07020	12737	E1
G191B2B	G230LB	11-11-06	13:00:20	216.0	obvp07030	12737	E1
G191B2B	G750L	11-11-06	13:10:17	1308.0	obvp07040	12737	
G191B2B	G230LB	12-10-14	18:00:31	468.0	oc3i14010	12813	E1
G191B2B	G430L	12-10-14	18:11:54	220.0	oc3i14020	12813	E1
G191B2B	G430L	12-10-14	19:01:02	220.0	oc3i14030	12813	
G191B2B	G750L	12-10-14	19:08:17	1100.0	oc3i14040	12813	HCR
G191B2B	G230LB	14-02-02	06:13:26	468.0	ocga06010	13599	
G191B2B	G430L	14-02-02	06:24:49	220.0	ocga06020	13599	
G191B2B	G430L	14-02-02	06:30:39	220.0	ocga06030	13599	E1
G191B2B	G750L	14-02-02	06:38:37	1058.0	ocga06040	13599	
G191B2B	G230LB	16-12-07	06:02:40	466.0	odck03010	14861	

Table 2. (cont'd)

Target	Mode	Date (YY-MM-DD)	Time (HH:MM:SS UT)	Exptime (s)	Obs ID	Prop ID	Flags:
G191B2B	G430L	16-12-07	06:14:01	216.0	odck03020	14861	
G191B2B	G430L	16-12-07	06:19:47	216.0	odck03030	14861	E1
G191B2B	G750L	16-12-07	07:32:53	1042.0	odck03040	14861	
G191B2B	G230LB	18-11-27	18:51:16	462.0	odud03010	15602	
G191B2B	G430L	18-11-27	19:02:33	214.0	odud03020	15602	
G191B2B	G430L	18-11-27	19:08:17	214.0	odud03030	15602	E1, HCR
G191B2B	G750L	18-11-27	20:00:24	1040.0	odud03040	15602	
G191B2B	G230LB	21-01-28	03:52:02	430.0	oejh03010	16436	
G191B2B	G430L	21-01-28	04:02:47	206.0	oejh03020	16436	
G191B2B	G430L	21-01-28	04:08:23	206.0	oejh03030	16436	E1
G191B2B	G750L	21-01-28	05:22:07	968.0	oejh03040	16436	
GD153	G230LB	97-05-21	10:18:00	600.0	o3tt42010	7063	
GD153	G430L	97-05-21	10:34:18	252.0	o3tt42020	7063	
GD153	G750L	97-05-21	11:31:25	3240.0	o3tt42040	7063	HCR
GD153	G230LB	97-05-28	06:53:29	600.0	o3tt43010	7063	
GD153	G430L	97-05-28	07:09:44	252.0	o3tt43020	7063	
GD153	G750L	97-05-28	08:04:35	3240.0	o3tt43040	7063	HCR
GD153	G230LB	97-06-04	11:28:46	600.0	o3tt44010	7063	
GD153	G430L	97-06-04	11:45:01	252.0	o3tt44020	7063	
GD153	G750L	97-06-04	12:41:08	3240.0	o3tt44040	7063	HCR
GD153	G230LB	97-06-10	22:22:09	600.0	o3tt45010	7063	
GD153	G430L	97-06-10	22:38:24	252.0	o3tt45020	7063	
GD153	G750L	97-06-10	23:33:17	3240.0	o3tt45040	7063	HCR
GD153	G230LB	97-06-18	04:24:17	600.0	o3tt46010	7063	
GD153	G430L	97-06-18	04:40:32	252.0	o3tt46020	7063	
GD153	G750L	97-06-18	05:46:23	2282.0	o3tt46040	7063	HCR
GD153	G230LB	97-06-25	04:11:40	600.0	o3tt47010	7063	
GD153	G430L	97-06-25	04:27:55	252.0	o3tt47020	7063	
GD153	G750L	97-06-25	05:31:49	2282.0	o3tt47040	7063	HCR
GD153	G230LB	97-07-01	12:03:44	600.0	o3tt48010	7063	
GD153	G430L	97-07-01	12:19:59	252.0	o3tt48020	7063	
GD153	G750L	97-07-01	13:11:51	2282.0	o3tt48040	7063	
GD153	G140L	97-07-13	04:44:14	187.1	o3zx080w0	7096	
GD153	G230L	97-07-13	04:56:19	187.1	o3zx080v0	7096	
GD153	G750L	98-05-17	20:42:46	900.0	o4a502020	7656	G1
GD153	G430L	98-05-17	21:04:01	240.0	o4a502030	7656	G1
GD153	G230LB	98-05-17	22:01:39	500.0	o4a502040	7656	G1
GD153	G230L	98-05-17	22:17:27	500.0	o4a502050	7656	
GD153	G140L	98-05-17	22:33:21	500.0	o4a502060	7656	
GD153	G230LB	97-11-12	01:28:59	400.0	o4d103010	7805	

Table 2. (cont'd)

Target	Mode	Date (YY-MM-DD)	Time (HH:MM:SS UT)	Exptime (s)	Obs ID	Prop ID	Flags:
GD153	G430L	97-11-12	01:41:54	180.0	o4d103020	7805	G1 Gain=1, P postarg used
GD153	G750L	97-11-12	01:51:09	740.0	o4d103030	7805	E1 52x2E1 Aperture,
GD153	G140L	98-07-15	11:07:48	204.0	o4vt100g0	8016	HCR high CR rejection
GD153	G140L	98-07-15	11:17:26	204.0	o4vt100f0	8016	P
GD153	G140L	98-07-15	11:28:19	204.0	o4vt100e0	8016	P
GD153	G140L	98-07-15	11:39:12	204.0	o4vt100d0	8016	P
GD153	G230L	98-07-15	12:32:53	288.0	o4vt100c0	8016	
GD153	G230L	98-07-15	12:47:05	288.0	o4vt100b0	8016	
GD153	G230L	98-07-15	12:59:22	288.0	o4vt100a0	8016	
GD153	G230L	98-07-15	13:11:39	288.0	o4vt10090	8016	
GD153	G140L	02-07-17	13:47:04	120.0	o6ig02080	8916	
GD153	G230L	02-07-17	13:56:29	180.0	o6ig02070	8916	
GD153	G140L	02-07-17	14:22:13	120.0	o6ig02050	8916	
GD153	G140L	01-12-11	22:21:36	120.0	o6ig03080	8916	
GD153	G230L	01-12-11	22:31:01	180.0	o6ig03070	8916	
GD153	G140L	01-12-11	22:56:45	120.0	o6ig03050	8916	
GD153	G140L	02-02-16	10:33:09	120.0	o6ig04080	8916	
GD153	G230L	02-02-16	10:42:34	180.0	o6ig04070	8916	
GD153	G140L	02-02-16	11:08:18	120.0	o6ig04050	8916	
GD153	G140L	02-06-17	07:52:12	120.0	o6ig11080	8916	
GD153	G230L	02-06-17	08:01:37	180.0	o6ig11070	8916	
GD153	G140L	02-06-17	08:27:21	120.0	o6ig11050	8916	
GD153	G230LB	04-01-05	08:32:59	425.0	o8v2020g0	10039	G1
GD153	G230LB	04-01-05	09:30:44	425.0	o8v2020f0	10039	E1, G1
GD153	G430L	04-01-05	09:44:11	220.0	o8v2020e0	10039	E1, G1
GD153	G430L	04-01-05	09:50:01	220.0	o8v2020d0	10039	G1
GD153	G750L	04-01-05	10:00:02	990.0	o8v2020c0	10039	G1
GD153	G140L	04-01-05	08:01:59	450.0	o8v2020b0	10039	
GD153	G230L	04-01-05	08:16:54	450.0	o8v2020a0	10039	
GD153	G140L	09-08-04	22:21:56	140.0	oa8d02010	11393	
GD153	G140L	09-08-06	16:00:41	170.0	oa9z05010	11403	
GD153	G230L	09-08-06	16:10:26	170.0	oa9z05020	11403	
GD153	G230L	11-01-13	23:38:56	595.0	obc402010	11999	
GD153	G230LB	11-01-14	00:06:09	656.0	obc402030	11999	
GD153	G430L	11-01-14	01:03:03	260.0	obc402040	11999	E1
GD153	G430L	11-01-14	01:09:33	260.0	obc402050	11999	HCR
GD153	G750L	11-01-14	01:17:28	1980.0	obc402060	11999	
GD153	G140L	11-01-13	23:53:29	596.0	obc402enq	11999	
GD153	G230L	13-01-01	15:54:07	595.0	obto10010	12682	
GD153	G230LB	13-01-01	16:21:18	656.0	obto10030	12682	

Table 2. (cont'd)

Target	Mode	Date (YY-MM-DD)	Time (HH:MM:SS UT)	Exptime (s)	Obs ID	Prop ID	Flags:
GD153	G430L	13-01-01	17:18:00	260.0	obto10040	12682	E1
GD153	G430L	13-01-01	17:24:30	260.0	obto10050	12682	
GD153	G750L	13-01-01	17:32:25	1980.0	obto10060	12682	
GD153	G140L	13-01-01	16:08:38	596.0	obto10qhq	12682	
GD153	G230L	13-01-01	23:53:01	592.0	oc5506010	13162	
GD153	G230LB	13-01-02	00:20:09	656.0	oc5506030	13162	
GD153	G430L	13-01-02	01:16:53	260.0	oc5506040	13162	E1
GD153	G430L	13-01-02	01:23:23	260.0	oc5506050	13162	
GD153	G750L	13-01-02	01:31:18	1974.0	oc5506060	13162	
GD153	G140L	13-01-02	00:07:29	596.0	oc5506rjq	13162	
GD153	G230L	14-01-20	14:31:02	592.0	ocga05010	13599	
GD153	G230LB	14-01-20	14:58:10	656.0	ocga05030	13599	
GD153	G430L	14-01-20	15:54:51	260.0	ocga05040	13599	E1
GD153	G430L	14-01-20	16:01:21	260.0	ocga05050	13599	
GD153	G750L	14-01-20	16:09:16	1974.0	ocga05060	13599	
GD153	G140L	14-01-20	14:45:30	596.0	ocga05euq	13599	
GD153	G230L	17-04-23	15:37:47	592.0	odck02010	14861	
GD153	G230LB	17-04-23	16:04:51	638.0	odck02030	14861	
GD153	G430L	17-04-23	17:03:08	254.0	odck02040	14861	E1
GD153	G430L	17-04-23	17:09:32	256.0	odck02050	14861	
GD153	G750L	17-04-23	17:17:23	1962.0	odck02060	14861	
GD153	G140L	17-04-23	15:52:15	592.0	odck02p2q	14861	
GD153	G230L	19-05-13	23:17:50	580.0	odud02010	15602	
GD153	G230LB	19-05-13	23:44:31	596.0	odud02030	15602	
GD153	G430L	19-05-14	00:44:29	254.0	odud02040	15602	E1
GD153	G430L	19-05-14	00:50:53	256.0	odud02050	15602	
GD153	G750L	19-05-14	00:58:44	1818.0	odud02060	15602	
GD153	G140L	19-05-13	23:32:06	581.0	odud02fpq	15602	
GD153	G230L	21-01-25	14:29:36	565.0	oehj02010	16436	
GD153	G230LB	21-01-25	14:55:47	566.0	oehj02030	16436	
GD153	G430L	21-01-25	15:56:48	250.0	oehj02040	16436	E1
GD153	G430L	21-01-25	16:03:08	250.0	oehj02050	16436	
GD153	G750L	21-01-25	16:10:53	1737.0	oehj02060	16436	
GD153	G140L	21-01-25	14:43:37	566.0	oehj02gyq	16436	
GD71	G750L	98-02-14	13:10:14	1980.0	o49x09010	7674	
GD71	G750L	98-03-17	12:59:21	1980.0	o49x10010	7674	
GD71	G750L	99-04-23	17:08:53	900.0	o4a520020	7656	G1
GD71	G430L	99-04-23	17:30:14	240.0	o4a520030	7656	G1
GD71	G230LB	99-04-23	18:27:22	500.0	o4a520040	7656	G1
GD71	G230L	99-04-23	18:43:05	500.0	o4a520050	7656	

Table 2. (cont'd)

Target	Mode	Date (YY-MM-DD)	Time (HH:MM:SS UT)	Exptime (s)	Obs ID	Prop ID	Flags:
GD71	G140L	99-04-23	18:59:14	500.0	o4a520060	7656	
GD71	G750L	98-11-04	08:10:14	900.0	o4a551020	7656	G1
GD71	G430L	98-11-04	08:31:29	240.0	o4a551030	7656	G1
GD71	G230LB	98-11-04	09:30:28	500.0	o4a551040	7656	G1
GD71	G230L	98-11-04	09:46:11	500.0	o4a551050	7656	
GD71	G140L	98-11-04	10:02:15	500.0	o4a551060	7656	
GD71	G140L	98-03-31	15:58:37	96.0	o4pg010l0	7917	
GD71	G140L	98-03-31	16:07:32	108.0	o4pg010k0	7917	
GD71	G140L	98-03-31	16:16:39	108.0	o4pg010j0	7917	P
GD71	G140L	98-03-31	17:06:45	108.0	o4pg010i0	7917	P
GD71	G140L	98-03-31	17:15:52	108.0	o4pg010h0	7917	P
GD71	G230L	98-03-31	17:27:20	216.0	o4pg010g0	7917	
GD71	G140L	98-04-27	06:15:01	108.0	o4sp01060	7932	
GD71	G140L	99-02-06	14:43:39	72.0	o53001080	7937	P
GD71	G140L	00-02-29	12:55:30	500.0	o5i001010	8421	P
GD71	G230L	00-02-29	13:10:45	500.0	o5i001020	8421	P
GD71	G230LB	00-02-29	13:24:09	500.0	o5i001030	8421	G1
GD71	G430L	00-02-29	14:20:21	240.0	o5i001040	8421	G1
GD71	G750L	00-02-29	14:30:42	900.0	o5i001050	8421	G1
GD71	G140L	00-03-01	06:40:22	108.0	o5i0020l0	8421	
GD71	G140L	00-03-01	06:48:04	108.0	o5i0020k0	8421	P
GD71	G140L	00-03-01	06:57:01	108.0	o5i0020j0	8421	P
GD71	G140L	00-03-01	07:05:58	108.0	o5i0020i0	8421	
GD71	G140L	00-03-01	07:14:55	108.0	o5i0020h0	8421	P
GD71	G230L	00-03-01	08:04:50	216.0	o5i0020g0	8421	
GD71	G430L	00-01-15	07:35:38	240.0	o61001010	8505	G1
GD71	G430L	00-01-15	07:41:06	240.0	o61001020	8505	
GD71	G230LB	00-01-15	07:51:27	700.0	o61001030	8505	G1
GD71	G750L	00-01-15	08:10:28	700.0	o61001040	8505	G1
GD71	G140L	00-01-15	09:19:23	250.0	o61001070	8505	
GD71	G230L	00-01-15	09:30:28	240.0	o61001080	8505	
GD71	G430L	00-01-18	06:39:11	240.0	o61002010	8505	G1
GD71	G230LB	00-01-18	06:49:32	700.0	o61002020	8505	G1
GD71	G750L	00-01-18	07:07:33	700.0	o61002030	8505	G1, HCR
GD71	G140L	00-01-18	08:27:02	250.0	o61002060	8505	P
GD71	G230L	00-01-18	08:38:07	250.0	o61002070	8505	
GD71	G430L	00-01-20	10:11:22	240.0	o61003010	8505	G1
GD71	G230LB	00-01-20	10:21:43	700.0	o61003020	8505	G1
GD71	G750L	00-01-20	10:39:44	700.0	o61003030	8505	G1, HCR
GD71	G140L	00-01-20	11:57:10	250.0	o61003060	8505	

Table 2. (cont'd)

Target	Mode	Date (YY-MM-DD)	Time (HH:MM:SS UT)	Exptime (s)	Obs ID	Prop ID	Flags:
GD71	G230L	00-01-20	12:08:15	250.0	o61003070	8505	
GD71	G430L	00-01-27	06:25:30	240.0	o61004010	8505	G1
GD71	G230LB	00-01-27	06:35:51	700.0	o61004020	8505	G1
GD71	G750L	00-01-27	06:53:52	700.0	o61004030	8505	G1, HCR
GD71	G140L	00-01-27	08:10:04	250.0	o61004060	8505	
GD71	G230L	00-01-27	08:21:09	250.0	o61004070	8505	
GD71	G430L	00-02-01	21:25:52	240.0	o61005010	8505	G1
GD71	G230LB	00-02-01	21:36:13	700.0	o61005020	8505	G1
GD71	G750L	00-02-01	21:54:14	700.0	o61005030	8505	G1
GD71	G140L	00-02-01	23:06:18	250.0	o61005060	8505	
GD71	G230L	00-02-01	23:17:23	250.0	o61005070	8505	
GD71	G430L	00-02-06	20:48:44	240.0	o61006010	8505	G1
GD71	G230LB	00-02-06	20:59:05	700.0	o61006020	8505	G1
GD71	G750L	00-02-06	21:17:06	700.0	o61006030	8505	G1, HCR
GD71	G140L	00-02-06	22:33:09	250.0	o61006060	8505	
GD71	G230L	00-02-06	22:44:14	250.0	o61006070	8505	
GD71	G230LB	01-12-07	05:41:27	310.0	o6ig010i0	8916	G1
GD71	G430L	01-12-07	05:52:58	150.0	o6ig010h0	8916	G1
GD71	G750L	01-12-07	06:01:49	440.0	o6ig010g0	8916	G1
GD71	G140L	01-12-07	02:48:39	450.0	o6ig010f0	8916	
GD71	G230L	01-12-07	03:03:34	500.0	o6ig010e0	8916	
GD71	G430L	03-10-24	01:29:17	180.0	o8v2010k0	10039	G1
GD71	G430L	03-10-24	01:34:27	180.0	o8v2010j0	10039	E1, G1
GD71	G750L	03-10-24	02:59:17	720.0	o8v2010i0	10039	G1
GD71	G140L	03-10-24	00:59:20	380.0	o8v2010h0	10039	
GD71	G230L	03-10-24	02:29:05	360.0	o8v2010e0	10039	
GD71	G230LB	03-10-24	04:42:17	350.0	o8v204040	10039	G1
GD71	G230LB	03-10-24	07:14:04	350.0	o8v204080	10039	E1, G1
GD71	G230L	10-03-10	03:38:31	595.0	obc401010	11999	
GD71	G230LB	10-03-10	04:05:48	660.0	obc401030	11999	
GD71	G430L	10-03-10	05:00:47	260.0	obc401040	11999	E1
GD71	G430L	10-03-10	05:07:16	260.0	obc401050	11999	
GD71	G750L	10-03-10	05:15:11	2010.0	obc401060	11999	
GD71	G140L	10-03-10	03:53:05	600.0	obc401m5q	11999	
GD71	G230L	11-11-02	21:01:37	595.0	obvp06010	12737	
GD71	G230LB	11-11-02	21:29:05	642.0	obvp06030	12737	E1
GD71	G430L	11-11-02	22:26:34	260.0	obvp06040	12737	E1
GD71	G430L	11-11-02	22:33:04	260.0	obvp06050	12737	
GD71	G750L	11-11-02	22:40:59	1980.0	obvp06060	12737	HCR
GD71	G140L	11-11-02	21:16:10	595.0	obvp06a8q	12737	

Table 2. (cont'd)

Target	Mode	Date (YY-MM-DD)	Time (HH:MM:SS UT)	Exptime (s)	Obs ID	Prop ID	Flags:
GD71	G230LB	13-02-12	12:32:00	600.0	oc3i15010	12813	E1
GD71	G430L	13-02-12	12:45:35	308.0	oc3i15020	12813	E1
GD71	G750L	13-02-12	12:55:00	1000.0	oc3i15030	12813	
GD71	G230L	14-02-05	15:52:07	595.0	ocga04010	13599	
GD71	G230LB	14-02-05	16:19:33	640.0	ocga04030	13599	E1
GD71	G430L	14-02-05	17:14:06	260.0	ocga04040	13599	E1
GD71	G430L	14-02-05	17:20:37	260.0	ocga04050	13599	
GD71	G750L	14-02-05	17:28:31	1974.0	ocga04060	13599	HCR
GD71	G140L	14-02-05	16:06:37	595.0	ocga04twq	13599	
GD71	G230L	17-01-17	22:15:52	595.0	odck01010	14861	
GD71	G230LB	17-01-17	22:43:18	616.0	odck01030	14861	E1
GD71	G430L	17-01-17	23:41:16	254.0	odck01040	14861	E1
GD71	G430L	17-01-17	23:47:40	256.0	odck01050	14861	
GD71	G750L	17-01-17	23:55:31	1962.0	odck01060	14861	HCR
GD71	G140L	17-01-17	22:30:23	595.0	odck01mwq	14861	
GD71	G230L	19-03-28	17:42:04	582.0	odud01010	15602	
GD71	G230LB	19-03-28	18:09:02	580.0	odud01030	15602	E1
GD71	G430L	19-03-28	19:08:46	254.0	odud01040	15602	E1
GD71	G430L	19-03-28	19:15:10	254.0	odud01050	15602	
GD71	G750L	19-03-28	19:22:59	1818.0	odud01060	15602	HCR
GD71	G140L	19-03-28	17:56:22	580.0	odud01r1q	15602	
GD71	G230L	21-03-16	21:28:52	560.0	oehj01010	16436	
GD71	G230LB	21-03-16	21:55:08	562.0	oehj01030	16436	E1
GD71	G430L	21-03-16	22:56:01	250.0	oehj01040	16436	E1
GD71	G430L	21-03-16	23:02:21	250.0	oehj01050	16436	
GD71	G750L	21-03-16	23:10:06	1737.0	oehj01060	16436	HCR
GD71	G140L	21-03-16	21:42:48	560.0	oehj01izq	16436	